
This is an electronic reprint of the original article.
This reprint may differ from the original in pagination and typographic detail.

Zaikovskii, Alexey; Yudin, Ivan; Kozlachkov, Dmitriy; Nartova, Anna; Fedorovskaya, Ekaterina
Gas pressure control of electric arc synthesis of composite Sn–SnO₂–C nanomaterials

Published in:
Vacuum

DOI:
[10.1016/j.vacuum.2021.110694](https://doi.org/10.1016/j.vacuum.2021.110694)

Published: 01/01/2022

Document Version
Peer-reviewed accepted author manuscript, also known as Final accepted manuscript or Post-print

Published under the following license:
CC BY-NC-ND

Please cite the original version:
Zaikovskii, A., Yudin, I., Kozlachkov, D., Nartova, A., & Fedorovskaya, E. (2022). Gas pressure control of electric arc synthesis of composite Sn–SnO₂–C nanomaterials. *Vacuum*, 195, Article 110694.
<https://doi.org/10.1016/j.vacuum.2021.110694>

This material is protected by copyright and other intellectual property rights, and duplication or sale of all or part of any of the repository collections is not permitted, except that material may be duplicated by you for your research use or educational purposes in electronic or print form. You must obtain permission for any other use. Electronic or print copies may not be offered, whether for sale or otherwise to anyone who is not an authorised user.

Gas pressure control of electric arc synthesis of composite ■ Sn–SnO₂–C nanomaterials



Alexey Zaikovski^{a,*} lexeyza@gmail.com, Ivan Yudin^a, Dmitriy Kozlachkov^a, Anna Nartova^b, Ekaterina Fedorovskaya^c

^aLaboratory of Rarefied Gases, Kutateladze Institute of Thermophysics SB RAS, 1 Lavrentyev Ave, Novosibirsk, 630090, Russian Federation

^bBoreskov Institute of Catalysis, Siberian Branch of the Russian Academy of Sciences, Novosibirsk, 630090, Russian Federation

^cResearch Group of Electrochemical Energy Conversion, Department of Chemistry, School of Chemical Engineering, Aalto University, P.O. Box 16100, FI-00076, Finland

*Corresponding author.

Abstract

It was found that the variation of a buffer gas pressure in the reactor chamber can control the structure of the synthesized materials during electric arc sputtering of composite Sn–C electrodes. The gas dynamic model calculated by the direct simulation Monte Carlo method shows that the buffer gas pressure affects the local parameters of tin and carbon vapor condensation. As a result, Core-shell Sn–SnO₂ nanoparticles packed in a carbon matrix with various structural properties have been synthesized. It has been found that an increase in the buffer gas pressure leads both to an increase in the average size of the synthesized nanoparticles and to the formation of a more disordered structure of carbon. In turn, the tin and carbon structure affects the electrochemical characteristics of the synthesized Sn–C composite as anode materials for lithium-ion batteries.

Keywords:

Nanoparticles, Tin, Carbon, Arc discharge, Direct simulation Monte-Carlo, Li-ion battery

1 Introduction

An electric arc discharge is one of types of plasma-chemical methods for nanomaterial synthesis. With the help of it, a macroscopic amount of fullerenes was experimentally obtained for the first time [1]. Also, carbon nanotubes were discovered for the first time in the synthesis products of the arc discharge [2]. This synthesis method was developed in the direction of the synthesis of graphene [3], metal and composite nanoparticles [4,5]. The structure and morphology of the synthesized materials are significantly influenced by external parameters of synthesis, such as the composition of the sputtered electrodes [6] and the discharge current [7]. Special attention should be paid to the influence of the buffer gas pressure on the structure of the resulting material.

The increase in the buffer gas pressure led to the order decreasing of the carbon structure formed during the electric arc sputtering of graphite electrodes [8]. With the increase in the oxygen pressure in the reactor chamber from 16 to 91 mbar, the fullerene content increased in the formed soot [9]. The increase in argon pressure supports decreasing of the defectiveness of carbon nanotubes produced in an arc discharge [10]. In number of works the effect of the gas pressure on the morphology and structure of materials obtained in a vacuum arc discharge were studied [11,12]. Despite numerous works related to the study of electric arc synthesis under different conditions, the physical processes affecting the structure of the formed material remain unclear. This paper presents the results of numerical simulation of gas-dynamic processes in the reactor chamber, which explain the effects of pressure on the morphology of the synthesized Sn–SnO₂–C nanomaterial.

In turn, tin nanomaterials have been found to be promising as anode material for the lithium-ion batteries [13]. Currently, commercial lithium-ion batteries use graphite as anode material. The use of graphite instead of metallic lithium is due to safety measures, since dendritic structures are formed at the anode of metallic lithium during numerous charge-discharge cycles, which can grow through the membrane and lead to a short circuit inside the battery, excessive heating and explosion [14]. In the case of using graphite, lithium ions are incorporated into the crystal lattice, forming the compound LiC₆ [15]. At the same time, dendritic structures are formed with a much less intensity. However, graphite anodes have a theoretical maximum specific capacity of only 372 mAhg⁻¹, which is much less than the value for metallic lithium, which has a theoretical capacity of approximately 3600 mAhg⁻¹. Materials made of elements from Group IV of the periodic table are considered to be a promising alternative to graphite [16]. One of these materials is tin, which has a theoretical specific capacity of 994 mAhg⁻¹ [17]. Tin oxide has a slightly lower capacity (782 mAhg⁻¹) [18]. However, when lithium ions are intercalated into the structure of tin, it increases its volume almost threefold. Numerous volumetric oscillations in the processes of battery charging and discharging lead to the destruction of the bulk tin structure [19], rapid material degradation, and electrode splitting off from the copper contact. The nanostructuring of the tin material helps to avoid this phenomenon. Moreover, tin nanoparticles should be separated from each other in order to prevent their coagulation. One of the solutions of the described problems can be the production of a composite material consisting of carbon nanostructure on which Sn or SnO₂ nanostructures are maintained [20–23].

This work presents the results of the study of methods for controlling the morphology of the synthesized Sn/SnO₂/C nanocomposite by means of varying the buffer gas pressure during electric arc synthesis.

2 Materials and methods

The calculations of the model of gas-dynamic processes in the reactor chamber were carried out by the method of direct simulation Monte-Carlo (DSMC) in an axisymmetric formulation [24]. The DSMC method is widely used to simulate rarefied gas flows. Model particles are used for calculations, each of which represents an ensemble of molecules with similar velocities and coordinates. Interaction of particles is a pairwise collision with a given interaction potential. In this work, the model of molecules with variable soft spheres (VSS-model) was adopted [24]. In the calculation model, the dimensions of the electrodes corresponded to the experimental ones: the diameter of the electrodes was 0.008 m, the distance between the electrodes corresponded to 0.004 m. The area between and around the electrodes was filled with helium at given pressure in the range from 1.3 to 80 mbar. The flow of atoms was set from the end of the anode based on the experimental data on the mass flow rate of the anode. Full absorption of tin and carbon particles was assumed on all surfaces. The solution was found by the method of establishment. The temperatures of the ends of the electrodes were set from the experimental data. The temperature distribution over the electrode surface was assumed linear, taking into account the water-cooled ends.

The experimental work of plasma-chemical synthesis was carried out using the electric arc reactor described in detail in Ref. [23]. The sprayed electrodes consisted of the cylindrical graphite rod with the coaxial cavity, which was tightly packed with the mixture of tin and graphite powders. In Ref. [23], the electric arc synthesis of composite Sn–C nanomaterials with different Sn content in the composition of sputtered electrodes has been carried out. The results of electrochemical studies of the synthesized materials showed that the materials synthesized with a Sn content of 40–60 wt% in the filling of electrodes have the best characteristics. In this work, the composition of the mixture corresponding to 60 wt% Sn and 40 wt% C was selected. The electric arc was ignited between the electrodes with current of 120A, the arc voltage was 25V. The pressure of helium used as a buffer gas varied from 1.3 to 266 mbar. The electric arc discharge led to heating and evaporation of the anode material, producing a gas-plasma mixture of

carbon, tin and helium, which formed a certain flow in the reactor chamber and deposited on the surfaces of the reactor chamber. Part of the anode evaporation products was deposited on the cathode surface, forming the cathode deposit. The rest was deposited on the inner surfaces of the reactor. The material was collected from the water-cooled screen located along the walls of the reactor and studied using transmission electron microscopy (TEM) and high resolution transmission electron microscopy (HRTEM) on a JEOL JEM-2010 instrument, energy dispersive X-ray spectroscopy (EDX) on EDAX console of scanning electron microscope Hitachi S-3400 N, X-ray diffractometry (XRD) on Bruker D8-Advance instrument, Raman spectroscopy on Horiba JobinYvon LabRAM HR Evolution Raman spectrometer instrument. The X-ray photoelectron spectroscopy (XPS) experiments were performed at a SPECS (Germany) spectrometer equipped with a hemispherical PHOIBOS-150-MCD-9 analyzer. Base pressure in analytic chamber was better than 1×10^{-7} Pa. The monochromatic Al K_{α} radiation ($h\nu = 1486.7$ eV) at 200 W was used as the primary excitation. The angle between normal line to the sample holder plane and analyzer axis (θ) was 0. The size of analyzed area is 3 mm in diameter. The spectrometer was calibrated using the Au $4f_{7/2}$ (binding energy (BE) is 84.0 eV) and Cu $2p_{3/2}$ (932.7 eV) peaks from metallic gold and copper foils [25]. During the XPS data analysis the Fermi edge as the energy reference was used. The binding energy values and the areas of XPS peaks were determined after Shirley background subtraction and analysis of line shapes [26]. For Sn 3d spectrum fitting ratio between spin-split components was fixed. Curves were fitted with Gaussian–Lorentzian functions for each XPS region. Spectral analysis and data processing were carried out with Peak 4.1 XPS [27]. The samples were fixed on the holder with the 3 M double sided adhesive copper conducting tape. The size of tape covered with the sample was ~ 0.01 m \times 0.01 m. Analysis position was optimized at the center of the sample.

Electrochemical studies of the synthesized materials were carried out using a BST8-MAcycler (Gelon group, China). For this, a slurry of 80% active materials (Sn–SnO₂–C), 10% SuperP powder (carbon black), and 10% polyvinylidene difluoride was prepared. The slurry was dissolved in N-methyl pyrrolidone (0.8 – 1 ml), which was spread over the surface of the copper foil and dried for 16 h at 80 °C. Next, the foil was cut into round electrodes. The electrochemical CR2032 Swagelok-type half-cell (Gelon group, China) was assembled in an argon glove box. The amount of the active material on the electrode surface was about 1 mg. The used electrolyte was 1 M LiPF₆ dissolved in a mixture (vol. 1: 1) of ethylene carbonate and dimethyl carbonate (Gelon group, China). Charge – discharge experiments were performed between 0.1 and 2.5 V versus Li|Li⁺ at a constant current density 100–1000 mA h g⁻¹ (galvanostatic mode) at room temperature.

3 Results and discussion

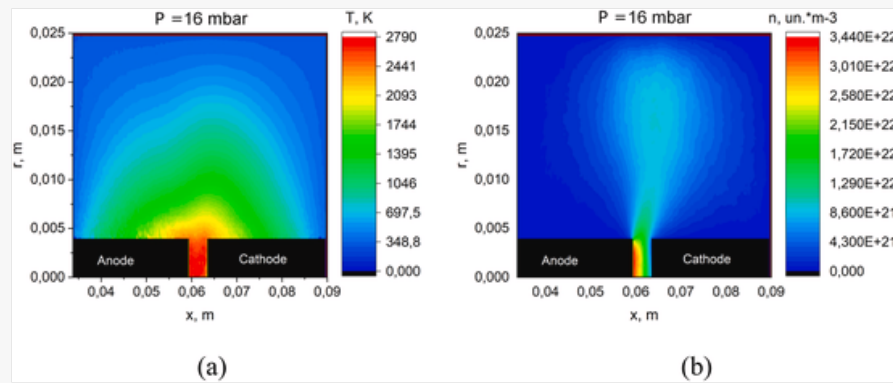
The electric arc discharge led to heating and evaporation of the anode material. Some of the evaporation products were deposited on the cathode surface. The other part escaped from the interelectrode gap, mixed with the buffer gas and formed a fan-shaped jet. In more detail, the gas-dynamic processes were modelled by the DSMC method. Earlier in Ref. [28], we have compared the gas temperature distribution in the reactor volume calculated by the DSMC method with the experimentally measured one. The calculated mass flow of the material deposited on the cathode has been also compared with the experimentally measured rate of increase in the mass of the cathode. The calculated and experimental results have shown good agreement. It has been concluded that the DSMC approach is a good tool for describing the processes occurring in the chamber of the electric arc reactor.

Fig. 1 shows the distribution patterns of the gas temperature and the concentration of carbon and tin atoms emitted from the anode surface during the electric arc discharge for helium pressure of 16 mbar.

 Images are optimised for fast web viewing. Click on the image to view the original version.

alt-text: Fig. 1

Fig. 1



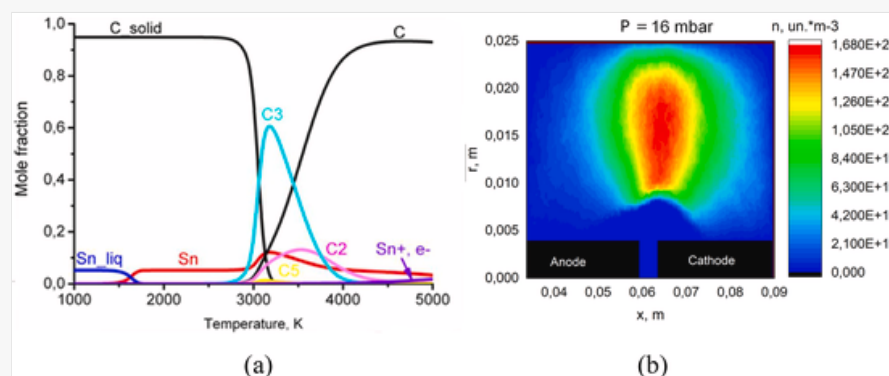
The distribution of gas temperature (a) and the distribution of the concentration of carbon and tin atoms (b) in the reactor chamber.

The equilibrium composition of the formed gas-plasma mixture was calculated taking into account the condition of quasi-neutrality, the law of conservation of mass and the condition of the minimum of Gibbs energy, using the NASA CEA software (Fig. 2a). When calculating the composition of the gas-plasma mixture, the following conditions were accepted: the initial composition of the reagents is 60 wt% Sn, 40% wt% C; pressure varies from 1.3 to 80 mbar: temperature varies from 1000 to 5000 K; the calculation includes ionized species as possible products; trace value was set as $1 \cdot 10^{-9}$; the calculated composition was presented in molar content.

 Images are optimised for fast web viewing. Click on the image to view the original version.

alt-text: Fig. 2

Fig. 2



The distribution of individual components of the gas-plasma mixture depending on the temperature (a) and the pattern of the distribution of liquid tin atoms in the reactor chamber (b).

The evaporation rate of the anode material makes it possible to estimate the temperature of the working surface of the anode using the Langmuir evaporation-condensation model [29]. The temperature is about 3000 K. At this temperature, the graphite component of the anode is dispersed mainly in the form of C_3 clusters and in a small amount in the form of C monatomic particles and C_2 diatomic particles. Tin at the given temperature exists only in the form of monoatomic vapor. Earlier in Ref. [30], the analysis has been carried out of materials formed at different distances from the arc discharge axis during sputtering of Sn-C electrodes. As the result of the study, the kinetic model of the formation of the structure of the composite Sn-C nanomaterial has been proposed. The outflow of the gas-plasma mixture from the interelectrode gap and its mixing with the buffer gas in the reactor chamber leads to cooling. At the first stage, at relatively high temperatures, atoms, dimers, and trimers of carbon condense, passing through the fullerene scenario, which includes the formation of linear chains, closed cycles, hemispheres and nuclei of fullerenes, as well as nuclei of a graphite structure. At lower temperatures, tin atoms begin to condense on the carbon structures present, forming tiny liquid droplets on the carbon surface. Collisions of carbon-tin particles with each other lead to the fusion of liquid tin, while carbon remains on the surface of the large tin droplet. The growth of the tin droplet size continues until carbon

completely covers the surface of the tin nanoparticle. Further collisions of the formed structures lead to aggregation into chains of particles, which are deposited on the inner surfaces of the reactor chamber.

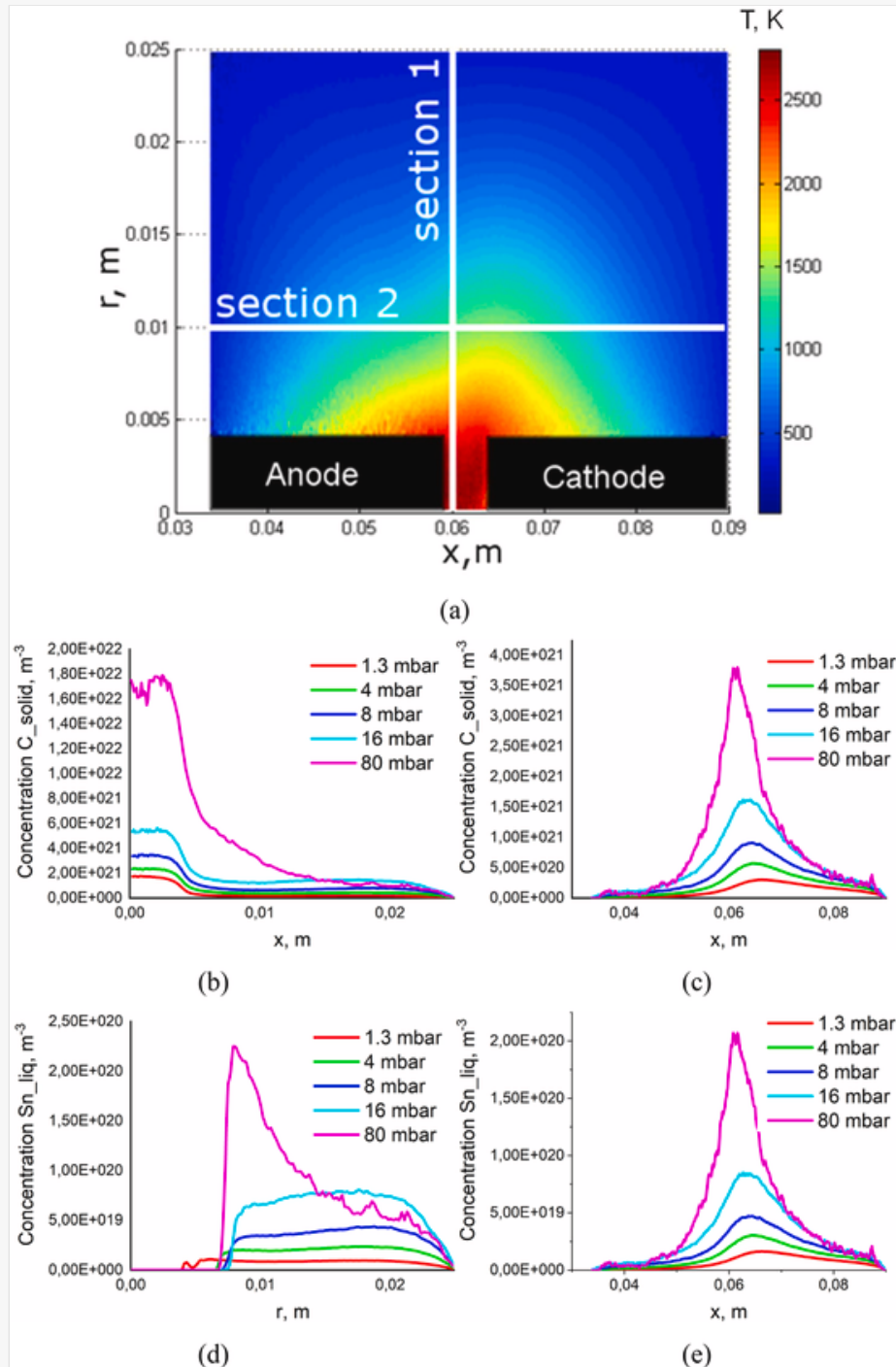
Using the patterns of the temperature distribution and the concentration of tin and carbon atoms in the reactor chamber, pictures of the concentration distribution of the individual components in the reactor chamber were constructed. Fig. 2b shows the distribution of liquid tin atoms in the reactor chamber.

Sections were selected perpendicularly and parallel to the arc discharge axis, along which the distributions of the atom concentration of condensed carbon and liquid tin were plotted for different helium pressures (Fig. 3a). As can be seen, carbon begins to condense already in the interelectrode gap itself and is predominantly located in the region no farther than 0.005 m from the discharge axis. Tin condensation begins at a distance of 0.005–0.008 m from the discharge, depending on the pressure of the buffer gas. As can be seen from the calculations, the increase in the helium pressure in the reactor chamber leads to the increase in the concentration of tin atoms. Previously it has been found that the increase in the concentration of tin leads to the increase in the size of synthesized nanoparticles [23]. Accordingly, the increase in the buffer gas pressure leads to the formation of larger nanoparticles. It is also worth noting that the increase in pressure snuggle the hot region closer to the discharge, which leads to the decrease in the tin condensation region and the corresponding increase in the concentration of tin atoms.

 Images are optimised for fast web viewing. Click on the image to view the original version.

alt-text: Fig. 3

Fig. 3



Selected sections (a) and distributions of condensed carbon atoms over the section parallel (b) and perpendicular (c) to the arc discharge axis and distribution of liquid tin atoms over the section parallel (d) and perpendicular (e) to the arc discharge axis.

On the other hand, the equilibrium composition calculated using the minimum Gibbs energy condition is the goal that the system tends to under given local conditions. It has been found that the conditions stimulating the process of carbon condensation are realized at distances of 0–0.005 m from the axis of the arc discharge. As shown by the DSMC method calculations, for all pressures of the buffer gas at these distances, the temperatures of helium and carbon particles are equal, which indicates the dissipation of the thermal energy of particles on helium molecules. The most interesting are the processes of tin condensation, which begin to occur at a distance of 0.005–0.008 m from the axis of the arc discharge, depending on the pressure of the buffer gas. At high pressures, the particles in the system experience a sufficient number of collisions to achieve a state of equilibrium. At low pressures, condensation processes are extended over an extended area in the reactor chamber. The sparseness of tin condensation processes is an additional factor that reduces the size of the formed tin nanoparticles.

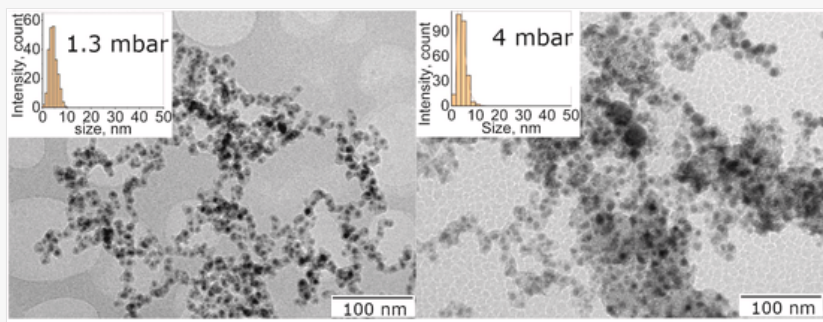
Structural studies of synthesized materials have shown that the electric arc sputtering results in synthesis of dense nanoparticles packed in a carbon matrix (Fig. 4). Most of the particles have the core-shell structure with the metal tin core and the amorphous tin oxide shell (Fig. 5a). Measurements of the sizes of nanoparticles in the carbon matrix shows

its log-normal distributions (Fig. 4), and the average size of nanoparticles increases with increasing pressure of the buffer gas in the reactor chamber (Fig. 5b), which qualitatively confirms the conclusions of the computational model.

 Images are optimised for fast web viewing. Click on the image to view the original version.

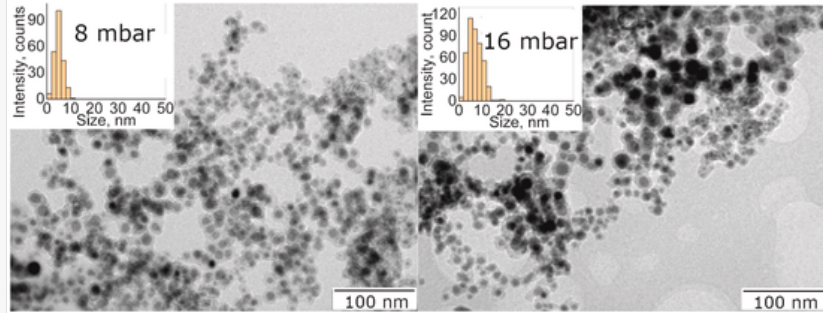
alt-text: Fig. 4

Fig. 4



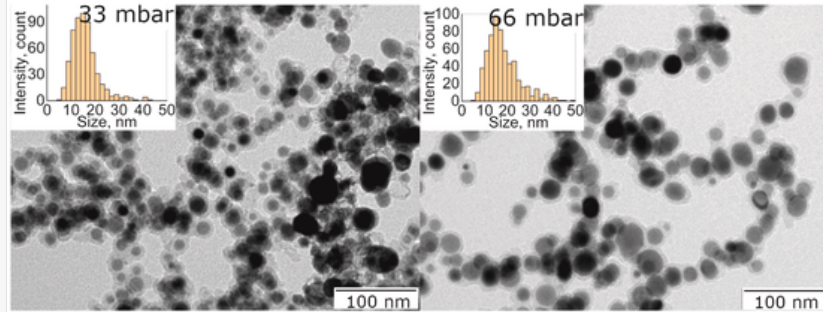
(a)

(b)



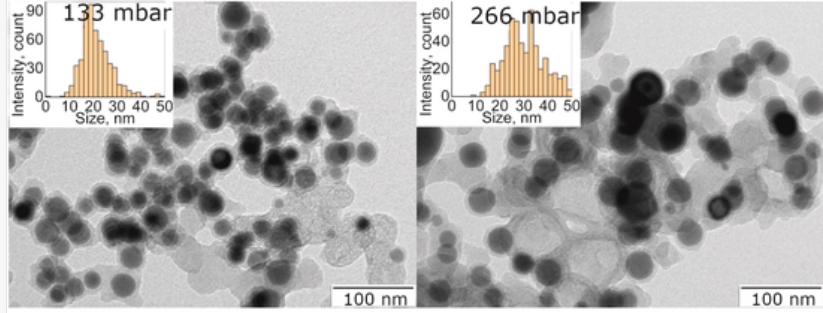
(c)

(d)



(e)

(f)



(g)

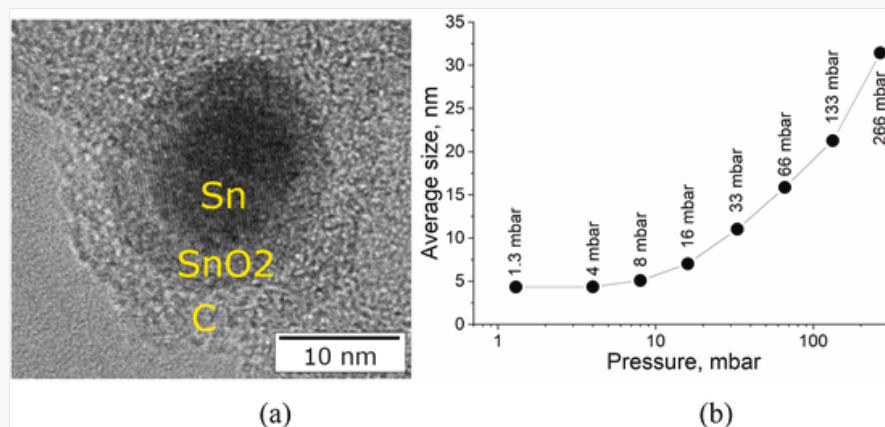
(h)

TEM images and histograms of nanoparticle size distributions for materials synthesized at buffer gas pressure 1.3 mbar (a), 4 mbar (b), 8 mbar (c), 16 mbar (d), 33 mbar (e), 66 mbar (f), 133 mbar (g) and 266 mbar (h).

 Images are optimised for fast web viewing. Click on the image to view the original version.

alt-text: Fig. 5

Fig. 5



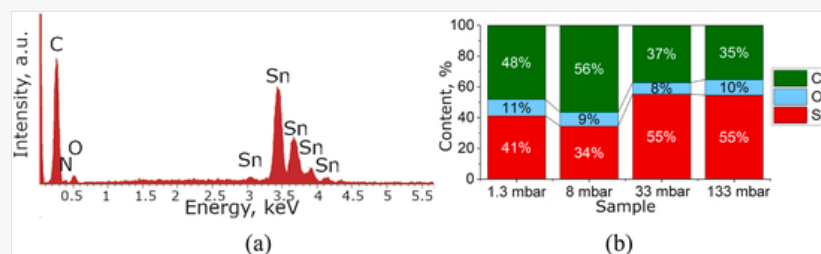
HRTEM image of Sn-SnO₂-C nanoparticle in material synthesized at buffer gas pressure 33 mbar (a) and the dependence of the average size of nanoparticles on the pressure of the buffer gas (b).

Analysis of the composition of the materials synthesized at different pressures demonstrates appearance of tin, carbon, and oxygen. Also, on the EDX spectra (Fig. 6a) there are small peaks of nitrogen, which is associated with air adsorption. The tin content varies from 34 to 55 wt%, carbon content varies from 35 to 56 wt% (Fig. 6b) and the oxygen content varies between 8 and 11 wt%.

 Images are optimised for fast web viewing. Click on the image to view the original version.

alt-text: Fig. 6

Fig. 6



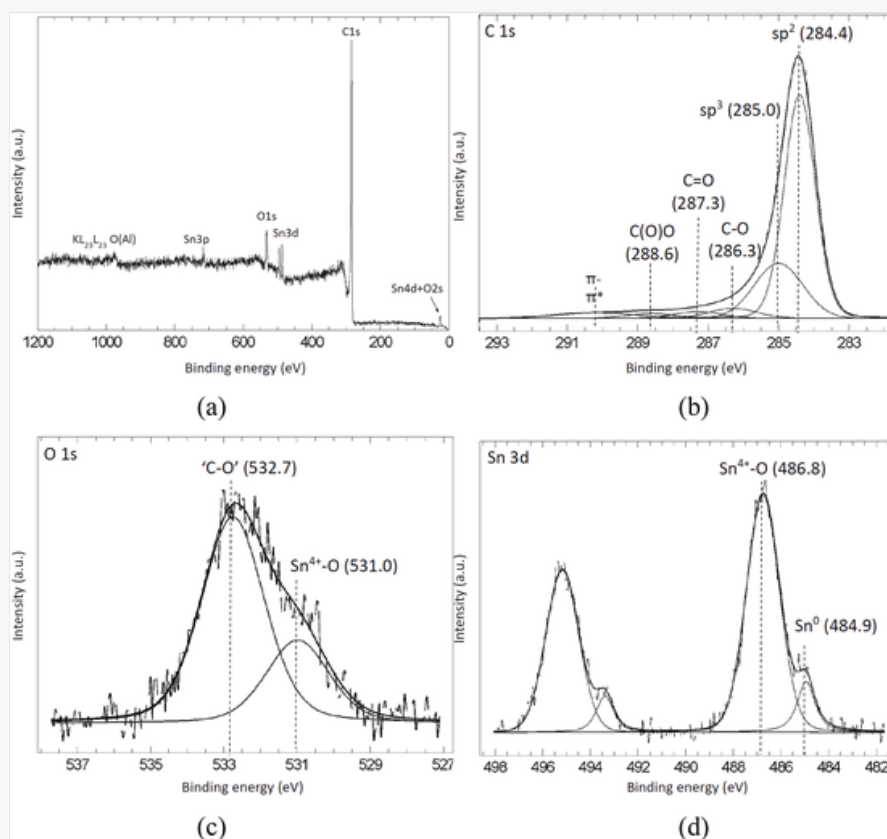
EDX - spectrum of material synthesized at 33 mbar (a) and elemental composition of materials synthesized at different pressures (b).

Oxygen atoms in the material are bonded with tin and carbon, which is confirmed by the results of XPS analysis (Fig. 7 b) [25,31,32]. However, the carbon atoms of the material predominantly are represented by unoxidized carbon atoms with sp^2 -, sp^3 -hybridization (Fig. 7c) [25,33-36]. According to analysis of the peak areas for oxide and metallic tin components portion of Sn⁰ is 13% within the depth of XPS analysis (Fig. 7d) [25,37-39]. It is explained by the large contribution of the oxide shell and the small contribution of the surface layer of the metallic core of the nanoparticles (Fig. 4b).

 Images are optimised for fast web viewing. Click on the image to view the original version.

alt-text: Fig. 7

Fig. 7



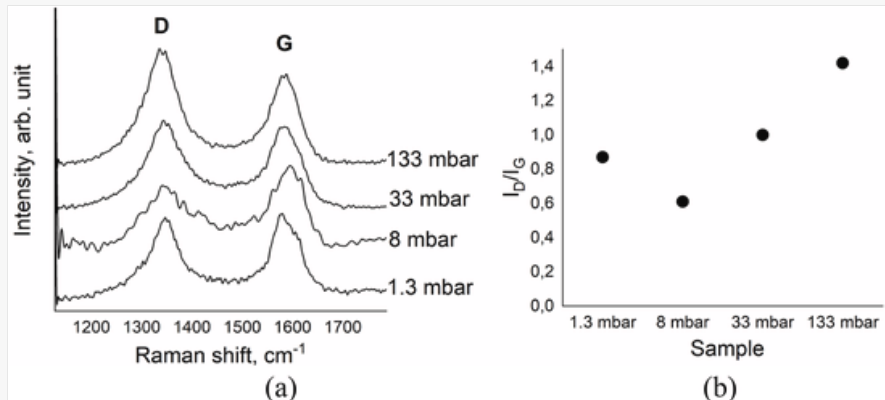
XPS spectrum of material synthesized at buffer gas pressure 33 mbar (a), peaks of tin (b), oxygen (c) and carbon (d).

Materials synthesized at 1.3, 8, 33 and 133 mbar were studied using Raman spectroscopy, which shows that carbon is presented in a highly disordered state, as evidenced by the intense D-peak in the spectra (Fig. 8a). The intensity ratio of the D-peak to G peak (I_D/I_G) takes a value of about 1, which indicates a highly disordered and amorphous structure of carbon [40]. Nevertheless, it can be noted that the increase in the buffer gas pressure from 8 to 133 mbar leads to the increase in the I_D/I_G ratio (Fig. 8b), which is related to the formation of a more defective and disordered carbon structure.

 Images are optimised for fast web viewing. Click on the image to view the original version.

alt-text: Fig. 8

Fig. 8



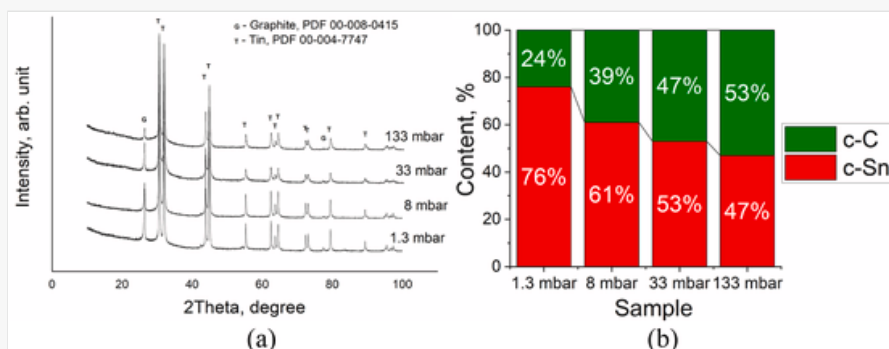
Raman spectra of the synthesized materials (a). Dependence of the I_D/I_G coefficient on the buffer gas pressure (b).

XRD spectra (Fig. 9a) shows that the crystal structure of the materials consists of carbon in the graphite form of $P6_3/mmc$ space group and crystalline tin of $I4_1/amd$ space group. The increase in the buffer gas pressure from 1.3 to 133 mbar leads to the increase in the crystal structure of tin from 24 to 53 wt% and the decrease in the crystal structure of carbon from 76 to 47 wt% (Fig. 9b). No clear peaks of tin oxide were detected on XRD spectra, which confirm the amorphous state of tin oxide in the shell of nanoparticles.

 Images are optimised for fast web viewing. Click on the image to view the original version.

alt-text: Fig. 9

Fig. 9

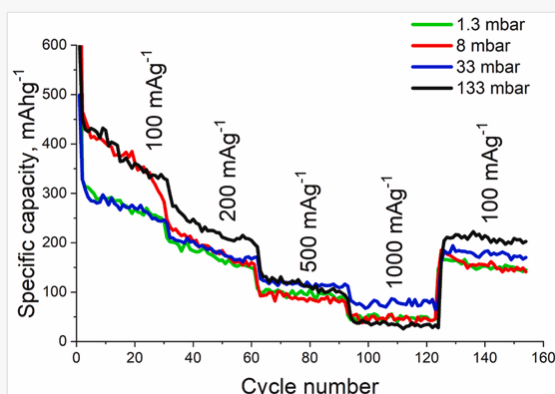


XRD patterns (a) and crystal composition (b) for materials synthesized at different pressures of the buffer gas.

Materials synthesized at 1.3, 8, 33, 133 mbar have been investigated as anode materials for lithium-ion batteries. After 160 charge-discharge cycles, the highest capacity at 100 mA h g^{-1} was shown by the material synthesized at pressure of 133 mbar, which has a capacity of 220 mA h g^{-1} (Fig. 10). This fact can be associated with the large size of Sn-SnO₂ particles, in which the thin surface layer of SnO₂ occupies the smaller part, and the Sn core occupies the largest part of the particle. Since Sn has a higher specific capacity (994 mA h g^{-1}) [17] than SnO₂ (782 mA h g^{-1}) [18], an increase in the Sn content leads to an increase in the specific capacity of the entire material.

alt-text: Fig. 10

Fig. 10



Specific capacity of Li-ion batteries with synthesized anode materials at various current densities.

On the other hand, large particles have a large diffusion path for lithium ions inside their structure, which negatively affects the specific capacity for high charge-discharge current densities of 500 and 1000 mA g^{-1} . Accordingly, materials synthesized at lower pressures have smaller particles, which show the higher specific capacity at high charge-discharge current densities of lithium-ion batteries.

4 Conclusion

Numerical modelling of gas-dynamic processes occurring during electric arc sputtering of Sn-C composite electrodes shows that an increase in the buffer gas pressure leads to an increase of resulting nanoparticle sizes. Structural studies of materials synthesized at different pressures of the buffer gas have qualitatively confirmed the growth of nanoparticle size with increasing pressure of the buffer gas. In this case, the synthesized material is core-shell Sn-SnO₂ particles packed in carbon matrix. The formation of the amorphous oxide layer on the metallic tin particles occurs upon contact of the material with air environment. Increasing the pressure of the buffer gas also leads to the formation of the more defective and disordered carbon structure, while the content of crystalline tin increases. The increase in the metal tin content in the synthesized materials with the buffer gas pressure growth is associated with the increase in the size of the tin metal core of the core-shell particles and the decrease in the volume fraction of the SnO₂ shell. This effect leads to the increase in the specific capacity of materials tested as anode materials for lithium-ion batteries. However, the increase in the size of nanoparticles leads to the decrease in the specific capacity at high charge-discharge currents of battery tests.

CRedit authorship contribution statement

Anna Nartova: Data curation, Formal analysis, Writing – review & editing, Software.

Declaration of competing interest

The authors declare that they have no known competing financial interests or personal relationships that could have appeared to influence the work reported in this paper.

Acknowledgments

The part of the work related to the arc-discharge plasma-chemical synthesis, structural and electrochemical analysis was supported by the [RSF](#) grant [20-79-00085](#). The part of the work related to the calculation and numerical simulation of the gas-dynamic processes was supported by the state contract with IT SBRAS.

References



- [1] Krätschmer W., Lamb L.D., Fostiropoulos K., et al., Solid C60: a new form of carbon, *Nature* 347 (1990) 354–358.
- [2] Iijima S., Helical microtubules of graphitic carbon, *Nature* 354 (1991) 56–58.
- [3] Subrahmanyam K.S., Panchakarla L.S., Govindaraj A., et al., Simple method of preparing graphene flakes by an arc-discharge method, *J. Phys. Chem. C* 13 (11) (2009) 4257–4259.
- [4] Saito Y., Okuda M., Yoshikawa T., et al., Correlation between volatility of rare-earth metals and encapsulation of their carbides in carbon nanocapsules, *J. Phys. Chem. Solid.* 98 (27) (1994) 6696–6698.
- [5] Scott J.H.J., Majetich S.A., Morphology, structure, and growth of nanoparticles produced in a carbon arc, *Phys. Rev. B* 52 (17) (1995) 12564–12571.
- [6] Smovzh D.V., Kostogrud I.A., Sakhapov S.Z., et al., The synthesis of few-layered graphene by the arc discharge sputtering of a Si-C electrode, *Carbon* 112 (2017) 97–102.
- [7] Zaikovskii A.V., Kardash T.Y., Kolesov B.A., et al., Graphene, SiC and Si nanostructures synthesis during quartz pyrolysis in arc-discharge plasma, *Phys. Status Solidi* 216 (2019) 1900079.
- [8] Zaikovskii A.V., Novopashin S.A., Electroconductive and magnetic properties of pure carbon soot produced in arc discharge: regimes of various buffer gas pressure, *Phys. Status Solidi* 214 (2017) 1700142.
- [9] Afanas'ev D.V., Bogdanov A.A., Dyuzhev G.A., et al., Production of fullerenes in an arc discharge in the presence of hydrogen and oxygen, *Tech. Phys.* 44 (1999) 1440–1443.
- [10] Essa I.M.A.L., Hermiz G.Y., Mohammed G.H., Structure of carbon nanotubes grown by arc-discharge technique under argon, N₂ and O₂ atmosphere at different conditions, *Int J CurrEng Technol* 5 (2) (2015) 834–839.
- [11] Fedorov L.Y., Karpov I.V., Ushakov A.V., et al., Influence of pressure and hydrocarbons on carbide formation in the plasma synthesis of TiC nanoparticles, *Inorg. Mater.* 51 (2015) 25–28.
- [12] Uschakov A.V., Karpov I.V., Lepeshev A.A., et al., Plasma-chemical synthesis of copper oxide nanoparticles in a low-pressure arc discharge, *Vacuum* 133 (2016) 25–30.
- [13] Mou H., Xiao W., Miao C., et al., Tin and tin compound materials as anodes in lithium-ion and sodium-ion batteries: a review, *Front Chem* 8 (2020) 141.
- [14] Frenck L., Sethi G.K., Maslyn J.A., et al., Factors that control the formation of dendrites and other morphologies on lithium metal anodes, *Front Energy Res* 7 (2019) 115.
- [15] Martin D., Martin S., Markus R., Phase formation and microstructure in lithium-carbon intercalation compounds during lithium uptake and release, *J. Power Sources* 353 (2017) 58–66.
- [16] Li W., Sun X., Yu Y., Si-, Ge-, Sn-based anode materials for lithium-ion batteries: from structure design to electrochemical performance, *Small Methods* 1 (3) (2017) 1600037.

- [17] Wang B., Luo B., Li X., et al., The dimensionality of Sn anodes in Li-ion batteries, *Mater. Today* 15 (12) (2012) 544–552.
- [18] Wang Y., Huang Z.X., Shi Y., et al., Designed hybrid nanostructure with catalytic effect: beyond the theoretical capacity of SnO₂ anode material for lithium ion batteries, *Sci. Rep.* 5 (1) (2015) 9164.
- [19] Edge J.S., O’Kane S., Prosser R., Lithium ion battery degradation: what you need to know, *Physiol. Chem. Phys.* 23 (2021) 8200–8221.
- [20] Li R., Xiao W., Miao C., et al., Sphere-like SnO₂/TiO₂ composites as high-performance anodes for lithium ion batteries, *Ceram* 45 (2019) 13530–13535.
- [21] Mou H., Chen S., Xiao W., et al., Encapsulating homogenous ultra-fine SnO₂/TiO₂ particles into carbon nanofibers through electrospinning as high-performance anodes for lithium-ion batteries, *Ceram* 47 (2021) 19945–19954.
- [22] Wu C.P., Xie K.X., He J.P., et al., SnO₂ quantum dots modified N-doped carbon as high-performance anode for lithium ion batteries by enhanced pseudocapacitance, *Rare Met.* 40 (2021) 48–56.
- [23] Zaikovskii A.V., Iurchenkova A.A., Kozlachkov D.V., et al., Effects of tin on the morphological and electrochemical properties of arc-discharge nanomaterials, *J. Occup. Med.* 73 (3) (2021) 847–855.
- [24] Bird G.A., *Molecular Gasdynamics and the Direct Simulation of Gas Flows*, (OUP): Clarendon Press, Oxford, 1994.
- [25] Moulder J.F., Stickle W.F., Sobol P.E., Kenneth K.D., in: Chastain J., King R.C. Jr. (Eds.), *Handbook of X-Ray Photoelectron Spectroscopy*, Physical Electronics, Inc., 1995.
- [26] Briggs D., Seah M.P., *Practical Surface Analysis by Auger and X-Ray Photoelectron Spectroscopy*, John Wiley & Sons. Inc, Chichester, 1983.
- [27] Using XPS PEAK version 4.1 . <https://xpspeak.software.informer.com/4.1/>, November 2000 .
- [28] Zaikovskii A., Yudin I., arc-discharge synthesis of composite carbon-tin nanomaterial for Li-ion battery anodes, 2020 7th International Congress on Energy Fluxes and Radiation Effects (EFRE), 2020, pp. 1160–1163 2020 Sep 13-25; Tomsk.
- [29] Langmuir I., Evaporation, condensation and adsorption, *J. Am. Chem. Soc.* 54 (7) (1932) 2798–2832.
- [30] Zaikovskii A., Novopashin S., Maltsev V., Tin–carbon nanomaterial formation in a helium atmosphere during arc-discharge, *RSC Adv.* 9 (2019) 36621–36630.
- [31] Beamson G., Briggs D., High resolution XPS of organic polymers: the scienta ESCA300 database, *J. Chem. Educ.* 70 (1) (1993) A25.
- [32] Badrinarayanan S., Mandale A.B., Gunjekar V.G., et al., Mechanism of high-temperature oxidation of tin selenide, *J. Mater. Sci.* 21 (1986) 3333–3338.
- [33] Smith M., Scudiero L., Espinal J., et al., Improving the deconvolution and interpretation of XPS spectra from chars by ab initio calculations, *Carbon* 110 (2016) 155–171.
- [34]

Briggs D., Beamson G., Primary and secondary oxygen-induced C1s binding energy shifts in x-ray photoelectron spectroscopy of polymers, *Anal. Chem.* 64 (15) (1992) 1729–1736.

- [35] Schmiege S.J., Belton D.N., Highly oriented pyrolytic graphite by XPS, *Surf. Sci. Spectra* 1 (1992) 333.
- [36] Bastl Z., X-ray photoelectron spectroscopic studies of palladium dispersed on carbon surfaces modified by ion beams and plasmatic oxidation, *Collect. Czech Chem. Commun.* 60 (3) (1995) 383–392.
- [37] Rubel M., Haasch R., Mrozek P., et al., Characterization of IrO₂/SnO₂ thin layers by electron and ion spectroscopies, *Vacuum* 45 (4) (1994) 423–427.
- [38] Parry-Jones A.C., Weightman P., Andrews P.T., The M4, 5N4, 5N4, 5 Auger spectra of Ag, Cd, in and Sn, *J. Phys. Chem.* 12 (8) (1979) 1587.
- [39] Stranick M.A., Moskwa A. SnO by XPS, *Surf. Sci. Spectra* 2 (45) (1993) 50.
- [40] Ferrari A.C., Robertson J., Interpretation of Raman spectra of disordered and amorphous carbon, *Phys. Rev. B* 61 (2000) 14095.

Highlights

- ~~A gas-dynamic model of the electric-arc plasma-chemical synthesis of the SnO₂-Sn-C nanocomposite was constructed using the Direct Simulation Monte Carlo method.~~ The gas-dynamic model of the electric-arc synthesis of the SnO₂-Sn-C nanocomposite was constructed using the DSMC method
 - ~~Numerical and experimental results show that an increase in the buffer gas pressure leads to an increase in the size of the synthesized tin nanoparticles.~~ Numerical and experimental results show that the gas pressure increase leads to the resulted particle size increase
 - ~~The structural characteristics of the synthesized SnO₂-Sn-C nanomaterials affect the electrochemical properties of materials as the anode material of lithium-ion batteries.~~ The structural characteristics of the synthesized SnO₂-Sn-C nanomaterials affect the electrochemical properties
-